Macroscopically Uniform Nanoperiod Alloy Multilayers Formed by Coupling of Electrodeposition with Current Oscillations

Shuji Nakanishi, Sho-ichiro Sakai, Tomoyuki Nagai, and Yoshihiro Nakato*

Division of Chemistry, Graduate School of Engineering Science, Osaka University, Toyonaka, Osaka 560-8531, Japan

Received: September 13, 2004; In Final Form: November 10, 2004

The electrodeposition from an acidic solution containing Cu^{2+}, Sn^{2+}, and a cationic surfactant gave a negative differential resistance (NDR) and a current oscillation in a narrow potential region of about 20 mV lying slightly more negative than the onset potential for Sn−Cu alloy deposition. Scanning Auger microscopic inspection has indicated that alloy films deposited during the oscillation have a clear alternate multilayer structure composed of two alloy layers of different compositions. The multilayer had the period of thickness of 40−90 nm and was uniform over a macroscopically wide area of about 1 mm × 1 mm. Detailed investigations have revealed that the NDR arises from adsorption of a cationic surfactant (acting as an inhibitor for diffusion of metal ions) on the alloy surface, and the oscillation comes from coupling of the NDR with the ohmic drop in the electrolyte.

Introduction

Self-organized formation of ordered micro- and nanostructures of metals and semiconductors at solid surfaces has attracted strong attention in view of nanoscience and nanotechnology.[1,2] The self-organization method has an advantage over the photolithography and surface probe method in that it meets both the conditions of atomic-scale fabrication and the adaptability of mass production. A number of studies has been reported on the self-organized formation of ordered structures, such as stripes, dot arrays, and target patterns, in the fields of nonlinear chemical reactions in homogeneous solutions[3−5] and at solid surfaces.[1,2,6−8] Electrochemical reactions with nonlinear kinetics also show a variety of self-organized spatiotemporal patterns at electrode surfaces.[9−13] Unfortunately, all dynamic patterns vanish when reactions have stopped. The only exception is a case of electrodeposition, in which ever-changing spatiotemporal patterns caused by reactions are recorded in a form of architecture of electrodeposits.

Schlitte et al. will be the first to report the formation of ordered architecture via an oscillatory electrodeposition.[14] They showed that the electrodeposition of Cu with a potential oscillation gave layered deposits.[14] Recently, Krastev et al. reported that the oscillatory electrodeposition of Sb and Ag gave similar layered deposits.[15,16] Interestingly, in this case, target patterns appeared at the surface of the deposits during the oscillation. The thickness of the layers in these examples was rather large, ranging in the order of 100 μm or more. On the other hand, Switzer et al. reported recently that the oscillatory electrodeposition of Cu in alkaline solutions gave alternate Cu and Cu_2O multilayers with the thickness of about 90 nm,[17,18] although they were not uniform, showing stratum-like waves in the cross section,[18] and less reproducible.[19,20] Unfortunately, no mechanism has been revealed yet in all the previous examples, which makes the control of layered structures quite difficult.

In the present paper, we report that the oscillatory electrodeposition of Cu−Sn alloy from an acidic solution of Cu^{2+} and Sn^{2+} produces nano-period layered deposits. The appearance of an oscillation in the electrodeposition of Cu−Sn alloy itself was reported before by Survila et al.,[21] but they did not report anything about the formation of a layered structure. A remarkable point of this system is that a macroscopically uniform nanoperiod multilayer is formed. Furthermore, we have, for the first time, succeeded in revealing the mechanism of the oscillation-induced layer formation. Some preliminary results were reported in a previous Letter.[22]

Experimental Procedures

A polycrystalline Au (99.99% in purity) disk 6 mm in diameter was used as the working electrode, together with a 10 × 10 mm^2 Pt plate as the counter electrode and an Ag|AgCl|sat. KCl electrode as the reference electrode. The Au electrode was polished with emery paper and diamond slurry and immersed in hot 1.5 M HNO_3 + 1.5 M H_2O_2 for 10 min to remove surface contamination.

The electrolyte was 0.60 M sulfuric acid containing $CuSO_4$ and $SnSO_4$ in various concentrations. The 0.5 M citric acid and 0.5 mM surfactant, such as Amiet-320 (Kao corp.), Amiet-302 (Kao), Triton-X 100 (ICN Biomedicals), C_{12}TAC (Tokyo-Kasei), SDS (Wako), and STS (Wako), were added to the electrolyte when needed. The chemical structures of these surfactants are shown in Figure 1, where Laprol-2402C used by Survila et al.[21] is included for reference. The electrolytes were prepared using special grade chemicals and pure water, the latter of which was obtained by purification of deionized water with a Milli-Q water purification system.

Current density (j) versus potential (U) curves and j versus time (t) curves were recorded digitally at 1 kHz with a data-storing system (instruNET, GW instruments). No correction was made for ohmic drops in the electrolyte in the present work. Analyses of layered structure and chemical composition of deposits were carried out with an apparatus (JEOL, JAMP-

* Corresponding auhor. Tel: +81-6-6850-6235; fax: +81-6-6850-6236; e-mail: nakato@chem.es.osaka-u.ac.jp.

10.1021/jp045876x CCC: $30.25 © 2005 American Chemical Society
Published on Web 01/13/2005

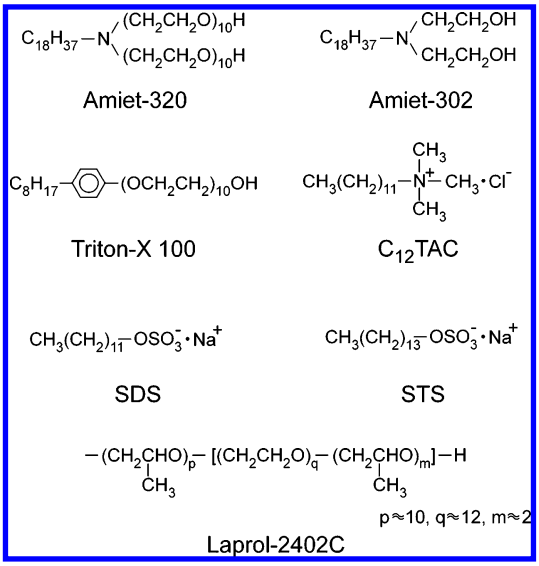

Figure 1. Chemical structures of surfactants used in the present work, except Laprol-2402C, which was used by Survila et al.[21]

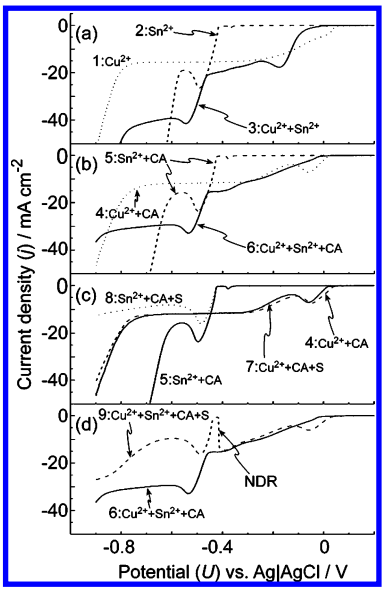

Figure 2. Curves 1−3: *j* vs *U* obtained in 0.6 M H_2SO_4 with (1) 0.15 M Cu^{2+}, (2) 0.15 M Sn^{2+}, and (3) 0.15 M Cu^{2+} + 0.15 M Sn^{2+}. Curves 4−6: *j* vs *U* in the same electrolytes as curves 1−3, respectively, except that 0.5 M citric acid (CA) was added. Curves 7−9: *j* vs *U* in the same electrolytes as curves 4−6, respectively, except that 0.5 mM Amiet-320 (*S*) was further added. The scan rate was 10 mV/s.

7820F) equipped with a scanning electron microscope (SEM), a scanning Auger electron microscope (scanning AEM), and an Ar-ion etching technique. The accelerated voltage in the scanning AEM was 10 kV.

Results

Figure 2 compares *j* versus *U* curves for metal deposition obtained in various electrolytes, all measured in the first negative scan. Curve 1 in Figure 2a shows *j* versus *U* in 0.15 M Cu^{2+} + 0.60 M H_2SO_4. The current for Cu deposition (or Cu^{2+} reduction) starts to flow at about +0.04 V. The diffusion-limited, potential-independent current for the Cu^{2+} reduction is reached at ca. −0.3 V, and hydrogen evolution starts at about −0.7 V. Curve 2 is *j* versus *U* in 0.15 M Sn^{2+} + 0.60 M H_2SO_4. The Sn deposition starts at −0.43 V, more negative than for the Cu deposition. The small cathodic peak appearing at −0.38 V is attributed to electrodeposition of Sn−Au alloy[23] because the Au working electrode is used in the present work.

Curve 3 is *j* versus *U* in 0.15 M Cu^{2+} + 0.15 M Sn^{2+} + 0.60 M H_2SO_4. Note that the curve is deviated from a simple sum of curves 1 and 2. In particular, the current in −0.30 to −0.45 V in curve 3 is higher (in the absolute value) than the diffusion-limited current for the Cu^{2+} reduction in curve 1, although the Sn^{2+} reduction does not occur at these potentials yet (curve 2). Shinohara et al. observed a similar increase in the current and reported, by X-ray diffraction (XRD) analysis, that the deposition in this potential range was ascribed to formation of γ-CuSn phase.[24] We also confirmed by Auger electron spectroscopy that Cu−Sn alloy was formed here.

Curves 4−6 in Figure 2b are *j* versus *U* in the same electrolytes as for curves 1−3, respectively, except that 0.5 M citric acid (CA) was added to obtain flattened surfaces for deposits,[25] as explained later. The addition of citric acid only affected the *j* versus *U* for the Cu deposition in a potential region above −0.35 V. We may note here that the *j* versus *U* in the solutions with Cu^{2+} and Sn^{2+} were somewhat scattered from experiment to experiment especially in a potential region above about −0.35 V. This is most probably because of the occurrence of some chemical reactions between Cu^{2+} and Sn^{2+} (such as $Cu^{2+} + Sn^{2+} \rightarrow Cu + Sn^{4+}$) in the solution and/or at the electrode surface. In the present work, however, we focus on the potential region from −0.30 to −0.45 V where a current oscillation appears as mentioned later; therefore, we do not discuss this problem anymore.

Curves 7−9 in Figure 2c,d are *j* versus *U* when 0.5 mM surfactant (Amiet-320) was further added to the electrolytes for curves 4−6, respectively. For the Cu^{2+} and the Sn^{2+} solutions (curves 7 and 8), the addition of the surfactant little affected the *j* versus *U*, only decreasing the Sn-deposition current in potentials below about −0.43 V. The decreased current suggests that the surfactant is adsorbed on the Sn surface and retards the Sn^{2+} diffusion. On the other hand, for the mixed (Cu^{2+} + Sn^{2+}) solution, the addition of the surfactant caused a drastic change in the *j* versus *U* (Figure 2d). Namely, an NDR, which was designated as NDR-2 in our previous Letter,[22] appeared in a narrow potential region of about 5 mV in the width near −0.42 V, where the Sn−Cu alloy is electrodeposited.

Another notable point in the surfactant-added solution is that a current oscillation appears when the *U* is kept constant in (and near) the potential region of this NDR. Figure 3a,b shows current oscillations observed in (0.15 M Cu^{2+} + 0.15 M Sn^{2+}) and (0.10 M Cu^{2+} + 0.10 M Sn^{2+}), respectively, both solutions containing commonly 0.6 M H_2SO_4, 0.5 mM Amiet-320, and 0.5 M citric acid. The oscillation period became longer and the waveform changed with an increase in the metal-ion concentrations. The potential regions in which the NDR and the oscillation appeared also shifted slightly with the metal-ion concentrations. All the surfactants in Figure 1, except SDS and STS, caused the appearance of both the NDR and the current oscillation, in nearly the same potential region as Amiet-320. Laprol-2402C was also reported[21] to give a similar NDR and oscillation. The surfactants in Figure 1, except SDS and STS, can be regarded as cationic surfactants because organic amines and ethers will be protonated in strongly acidic 0.6 M H_2SO_4 solutions, whereas SDS and STS are anionic surfactants. The previous results thus indicate that the appearances of the NDR and current oscillation are caused only by cationic surfactants. Both the NDR and the oscillation appear even in the absence of citric acid, but the oscillation becomes stable in the presence of citric acid, continuing for about 30 min.

The structure of alloy films deposited during the current oscillation was investigated by SEM and scanning AEM. Figure

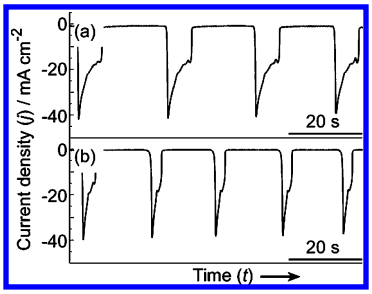

Figure 3. Time courses of current oscillations in (a) 0.15 M $CuSO_4$ + 0.15 M $SnSO_4$ and (b) 0.10 M $CuSO_4$ + 0.10 M $SnSO_4$, both containing 0.6 M H_2SO_4 + 0.5 M citric acid + 0.5 mM Amiet-320.

4a schematically illustrates the procedure of sample preparation. The deposited film was etched with an Ar^+-ion beam with an energy of 1 keV and a current of 20 mA in a vacuum, with the film being rotated. This procedure gave a bowl-shaped hollow of about 1 mm in the diameter at the bottom, together with a slanting cross section of the deposited film. Figure 4b shows an SEM image (top view) of a sample thus prepared. Uniform concentric rings of gray and black colors in the region of the slanting cross-section clearly indicate the formation of a quite uniform layered structure spreading over a macroscopically wide range of 1 × 1 mm. We confirmed that a set of the gray and black layers (one period of the multilayer) was formed by one cycle of the oscillation, by observing that the number of the sets in the deposited film agreed with the number of cycles of the oscillation during which the deposited film was obtained. On the basis of this fact, the average thickness of one set (one period of the superlattice) was estimated from the electricity flowing during the oscillation to be about 50 nm.

Figure 4c compares the expanded SEM image in the region of the slanting cross section with the profile (white curve) of the atomic ratio [Cu/(Cu + Sn)] in this region, the latter of which was obtained from the peak areas of scanning AEM corrected for the sensitivity factors. We can see that Cu is rich in the black layer, whereas Sn is rich in the gray layer.

Figure 5a,b shows Auger depth profiles for deposited films obtained during the oscillations of Figure 3a,b, respectively. The thickness of one period of the multilayer, calculated from the sputter time in the Ar^+-ion sputtering, with the sputtering rate for the deposited Cu−Sn alloy being assumed to be the same as that reported for Cu metal (10.4 nm/min under the present conditions of an Ar^+-ion current of 20 mA and energy of 1 keV), is shown in Figure 5. The same quantity was also calculated from the electricity flowing during the oscillation. The latter method gave the values of about 87 and 38 nm for the deposited films of Figure 5a,b, respectively, in good agreement with those obtained from the sputter time.

To clarify the electrodeposition process in the potential region of the current oscillation, we also observed the depth profile for a deposited film obtained when U was scanned from +0.1 to −0.5 V (see Figure 6a) in the same solution as for curve 9 of Figure 2 (0.15 M Cu^{2+} + 0.15 M Sn^{2+} + 0.6 M H_2SO_4 + 0.5 mM Amiet 320 + 0.5 M citric acid). Figure 6b shows observed depth profiles for the Cu and Sn contents, with the distance measured from the surface of the Au substrate. The distance was calculated from the sputter time in the same way as stated previously. The result indicates that Cu is first deposited to the thickness of 126 nm, and then Sn begins to be deposited. The Sn content increases with the increasing thickness. Figure 6c schematically illustrates the distributions of the Cu and Sn contents in the deposited film. A calculation shows that the deposition of a 126 nm Cu layer needs the electricity

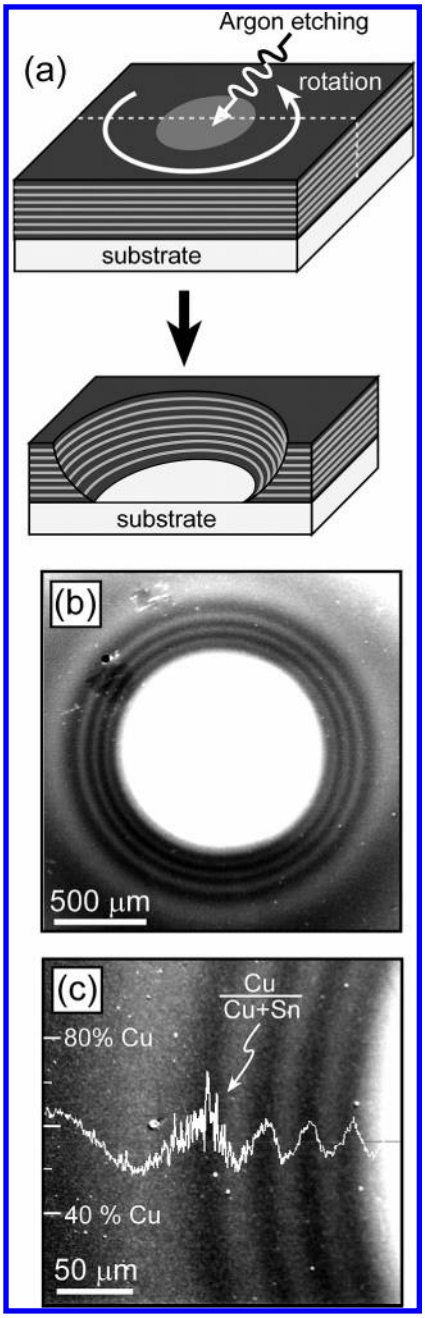

Figure 4. (a) Schematic illustration of sample preparation for SEM and AEM analyses. (b) SEM (top view) of a bowl-shaped hollow with a slanting cross section, prepared in the deposited alloy film by Ar^+-ion etching. (c) Expanded SEM image, compared with a distribution of the atomic ratio [Cu(Cu + Sn)] obtained with a scanning AEM.

(Q) of 340 mC cm^{-2}. This quantity (Q) flows when U is scanned down to −0.3 V (the shaded area of Figure 6a). This implies that Sn begins to be deposited at −0.3 V, in agreement with the result of curve 3 in Figure 2. We can also conclude from Figure 6b that the Sn content in the deposited Cu−Sn alloy film increases with the negative shift in U.

Finally, we may note that the addition of 0.5 M citric acid to the solution affects strongly the morphology of the surface of the deposited film, although it little affects the $j-U$ curve in the potential region of the NDR, as mentioned earlier. Citric acid was used as a reagent to obtain a flattened surface for NiP−alloy electrodeposition,[25] although the mechanism was not clarified. Uniform concentric rings such as those shown in Figure 4b can only be obtained in the presence of citric acid, indicating that it works as a flattening reagent also in the CuSn−

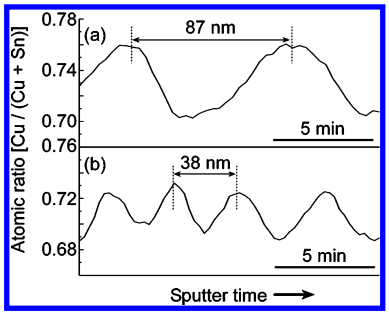

Figure 5. Auger depth profiles for two kinds of deposited films, obtained by combination with the Ar^+-ion sputtering technique. Electrolytes (and externally applied U): (a) 0.15 M $CuSO_4$ + 0.15 M $SnSO_4$ (−432 mV) and (b) 0.10 M $CuSO_4$ + 0.10 M $SnSO_4$ (−418 mV), both containing 0.6 M H_2SO_4, 0.5 citric acid, and 0.5 mM Amiet-320.

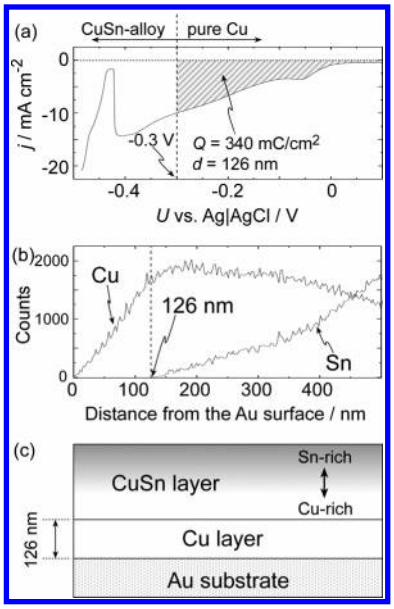

Figure 6. (a) j vs U observed when U was scanned from +0.1 to −0.6 V at a constant rate of 5 mV/s. (b) Depth profiles for Cu and Sn in the alloy film deposited during the above scan (a). (c) Schematic illustration of the Cu and Sn contents in the deposited film, drawn from the above result (b).

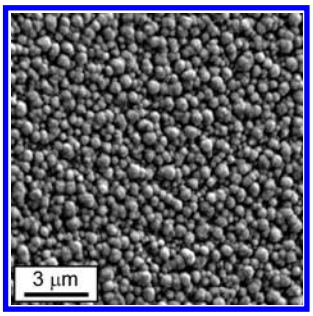

Figure 7. Surface SEM of the Cu−Sn alloy film, electrodeposited without 0.5 M citric acid in 0.15 M $CuSO_4$ + 0.15 M $SnSO_4$ + 0.6 M H_2SO_4 + 0.5 mM Amiet-320. The applied potential was −0.42 V.

alloy electrodeposition. The surface of deposited films in the absence of citric acid was quite rough, composed of many particles with the diameter of several hundreds nanometers, as shown in Figure 7.

Discussion

The experimental results show that the present deposition system gives an interesting example of formation of macroscopically uniform nanoperiod alloy multilayers by oscillatory electrodeposition. To reveal the mechanisms for the oscillation and multilayer formation is quite important to control and modify (or further develop) the multilayer structure. As mentioned in the Introduction, no mechanism has been clarified for previously reported examples[14−18] of the formation of oscillation-induced layered deposits.

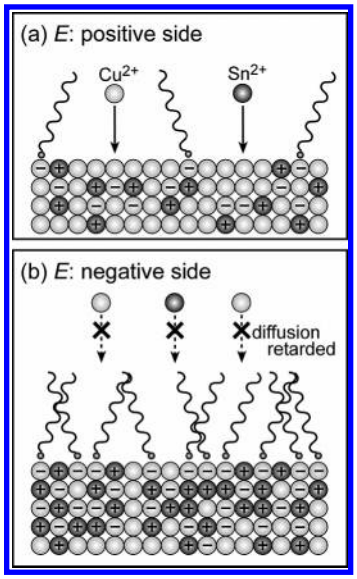

Figure 8. Schematic cross-sectional views of the surfaces of alloy deposits in (a) high-current (or positive E) and (b) low-current (or negative E) stages of the current oscillation. Gray circle Cu; black circle Sn; and + and − partial electric charges induced by a difference in the electronegativity between Sn and Cu.

According to recent theoretical work on electrochemical oscillations, there are four[26−29] (or five[30]) types of mechanisms in their appearance, from type I to type IV (or V). The current oscillation in the present work can be classified into type III oscillators (called NDR oscillators),[26] as explained next. In general, the coupling of an NDR in the j versus U curve with the ohmic drop in the electrolyte causes an autocatalytic process in the true electrode potential (or Helmholtz double layer potential), E, which leads to bistability of the system. A current oscillation appears when another slow process, having an action to push back the autocatalytic change in E, exists in the system. In most cases, diffusion of an electroactive species to the electrode surface acts as such a slow process. This is the mechanism of type III (NDR) oscillators, and the current oscillation in the present work can be explained by this mechanism.

Let us first consider the origin of the NDR observed in Figure 2d, from which the current oscillation appears. We should note that the NDR appears in the potential region where the Cu−Sn alloy is deposited. In addition, it appears only in the presence of a cationic surfactant and not in the presence of an anionic surfactant. This fact strongly suggests that the NDR arises from electrostatic adsorption of a cationic surfactant on a (negatively polarized) Sn−Cu alloy (deposit) surface because the adsorption will retard the diffusion of electroactive metal ions (Cu^{2+} and Sn^{2+}) to the alloy surface and thus decrease j. We mentioned in the preceding section that the Sn content in the Sn−Cu alloy increased with a negative shift in U (Figure 6), although the Cu content was still dominant (Figures 4c and 5). In such a situation, we can assume that a negatively polarized surface is formed by a difference in the electronegativity between Cu and Sn atoms, as schematically shown in Figure 8. The negative polarization at the surface, and hence the amount of a cationic

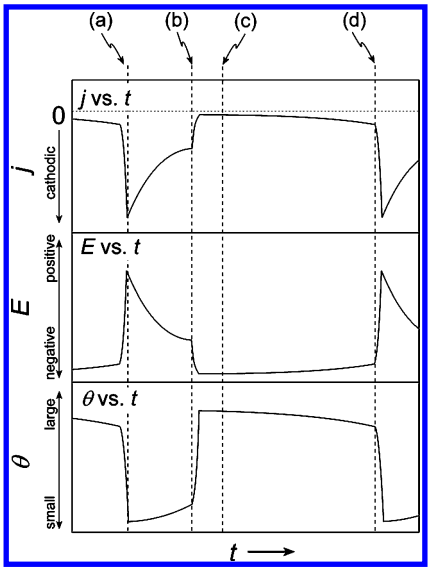

Figure 9. Schematic illustrations of expected j vs t, E vs t, and θ vs t.

surfactant adsorbed on it, will increase with an increase in the Sn content (i.e., with a negative shift in U).

On the basis of the previous argument, we can now explain the mechanism for the current oscillation and the multilayer formation. First note that U is kept constant externally with a potentiostat in the present case. Let us start to consider a (absolutely) high-current stage of the current oscillation. In this stage, the true electrode potential (or Helmholtz double layer potential), E, is much more positive than U because E is given by $E = U - jAR$, where A is the electrode area, R is the resistance of the solution between the electrode surface and the reference electrode, and j is taken as negative for the reduction current. This implies that, even if U is kept in the region of the NDR, E is much more positive than U, and hence the coverage (θ) of the adsorbed surfactant in this stage is small. Thus, effective diffusion of Cu^{2+} and Sn^{2+} to the electrode surface occurs without retardation, which leads to a high j value due to active electrodeposition of the Cu−Sn alloy (stage a in Figure 9).

The active alloy deposition, however, causes decreases in the surface concentrations of Cu^{2+} and Sn^{2+} ions (hereafter denoted as C_{Cu2+} and C_{Sn2+}) owing to their slow diffusion from the solution bulk. This leads to a gradual decrease in j (in the absolute value) and thus to a decrease in the ohmic drop and a negative shift in E. The negative shift in E, in turn, leads to an increase in θ. Thus, the j decreases (stage b) owing to a decrease in the diffusion of Cu^{2+} and Sn^{2+} to the electrode surface, and the system goes to a low-current stage, accompanied by a negative shift in E.

In the low-current stage (stage c), only slow deposition (or slow reduction of Cu^{2+} and Sn^{2+}) occurs at vacant sites (atomic pinholes); thus, C_{Cu2+} and C_{Sn2+} gradually increase by diffusion from the solution bulk. The increase in C_{Cu2+} and C_{Sn2+} induces an increase in j and thus causes a positive shift in E (and a decrease in θ). When E is shifted to the positive, the j increases (stage d) owing to an increase in the diffusion of Cu^{2+} and Sn^{2+}, and the high-current stage is restored again.

The alternate-multilayer formation in the alloy deposit can be explained on the basis of the previous mechanism. First, we have to note that the j value in the low-current stage is very low; hence, this stage hardly contributes to the alloy formation. In the high-current stage, the E shifts gradually to the negative with time, as seen in Figure 9, and the Sn content in the alloy deposit increases with this negative shift in E (Figure 6). Accordingly, one period of the multilayer is formed by one cycle of the current oscillation.

The previous mechanism can be used to control the oscillation behavior and the multilayer structure. In fact, a change in the concentrations of Cu^{2+} and Sn^{2+} affect the duration time of the high-current state between stages a and b, as seen in Figure 3, which is in good agreement with the previous mechanism.

In conclusion, the present work has revealed that the Cu−Sn alloy deposition from an acidic ($Cu^{2+} + Sn^{2+}$) solution in the presence of a cationic surfactant gives an NDR-type current oscillation and formation of macroscopically uniform nanoperiod alloy multilayers. The present work has also succeeded in clarifying the mechanism for the oscillation and multilayer formation. This is very important to tune the oscillatory waveform as well as the multilayer structure on a nanometer scale. The mechanism will generally be applicable to the electrodeposition reaction with an NDR and is expected to contribute for formations of other layered structures. Thus, further studies along this line will provide a novel way to prepare a variety of nanostructures by use of the oscillation−electrodeposition coupling.

Acknowledgment. The authors thank the Core Research for Evolutional Science and Technology (CREST) program of the Japan Science and Technology Agency (JST) for financial support. This work was also partly supported by a Grant in Aid of the Ministry of Education, Culture, Sport, Science, and Technology (MEXT) for scientific research, the Kao Foundation for Arts and Science, and the Murata Science Foundation.

References and Notes

(1) Notzel, R.; Temmyo, J.; Tamamura, T. *Nature* **1994**, *369*, 131.
(2) Kim, S. O.; Solak, H. H.; Stoykovich, M. P.; Ferrier, N. J.; de Pablo, J. J.; Nealey, P. F. *Nature* **2003**, *424*, 411.
(3) Vanag, V. K.; Yang, L.; Dolnik, M.; Zhabotinsky, A. M.; Epstein, I. R. *Nature* **2000**, *406*, 389.
(4) Epstein, I. R. *Nature* **1984**, *307*, 692.
(5) Orban, M.; Dekepper, P.; Epstein, I. R.; Kustin, K. *Nature* **1981**, *292*, 816.
(6) Plass, R.; Last, J. A.; Bartelt, N. C.; Kellogg, G. L. *Nature* **2001**, *412*, 875.
(7) Frost, F.; Schindler, A.; Bigl, F. *Phys. Rev. Lett.* **2000**, *85*, 4116.
(8) Pohl, K.; Bartelt, M. C.; de la Figuera, J.; Bartelt, N. C.; Hrbek, J.; Hwang, R. Q. *Nature* **1999**, *397*, 238.
(9) Li, Y. J.; Oslonovitch, J.; Mazouz, N.; Plenge, F.; Krischer, K.; Ertl, G. *Science* **2001**, *291*, 2395.
(10) Lev, O.; Sheintuch, M.; Pisemen, L. M.; Yarnitzky, C. *Nature* **1988**, *336*, 458.
(11) Krischer, K. *J. Electroanal. Chem.* **2001**, *501*, 1.
(12) Krischer, K.; Mazouz, N.; Grauel, P. *Angew. Chem.—Intl. Ed.* **2001**, *40*, 851.
(13) Christoph, J.; Eiswirth, M. *Chaos* **2002**, *12*, 215.
(14) Schlitte, F. w.; Eichkorn, G.; Fischer, H. *Electrochim. Acta* **1968**, *13*, 2063.
(15) Krastev, I.; Koper, M. T. M. *Phys. A* **1995**, *213*, 199.
(16) Nakabayashi, S.; Krastev, I.; Aogaki, R.; Inokuma, K. *Chem. Phys. Lett.* **1998**, *294*, 204.
(17) Switzer, J. A.; Hung, C. J.; Huang, L. Y.; Switzer, E. R.; Kammler, D. R.; Golden, T. D.; Bohannan, E. W. *J. Am. Chem. Soc.* **1998**, *120*, 3530.
(18) Bohannan, E. W.; Huang, L. Y.; Miller, F. S.; Shumsky, M. G.; Switzer, J. A. *Langmuir* **1999**, *15*, 813.
(19) Bonnefont, A.; Kostecki, R.; McLarnon, F.; Arrayet, J. C.; Servant, L.; Argoul, F. *J. Electrochem. Soc.* **1999**, *146*, 4101.
(20) Leopold, S.; Schuchert, I. U.; Lu, J.; Molares, M. E. T.; Herranen, M.; Carlsson, J. O. *Electrochim. Acta* **2002**, *47*, 4393.
(21) Survila, A.; Mockus, Z.; Juskenas, R. *Electrochim. Acta* **1998**, *43*, 909.
(22) Sakai, S.; Nakanishi, S.; Fukami, K.; Nakato, Y. *Chem. Lett.* **2002**, 640.
(23) Mao, B. W.; Tang, J.; Randler, R. *Langmuir* **2002**, *18*, 5329.

(24) Shinohara, N.; Arai, S.; Kaneko, N.; Wakabayashi, S. *Hyoumen Gijyutsu (Japanese)* **2001**, *52*, 693.
(25) Miyake, T.; Kume, M.; Yamaguchi, K.; Dinesh, P. A.; Minoura, H. *Thin Solid Films* **2001**, *397*, 83.
(26) Strasser, P.; Eiswirth, M.; Koper, M. T. M. *J. Electroanal. Chem.* **1999**, *478*, 50.
(27) Koper, M. T. M.; Sluyters, J. H. *J. Electroanal. Chem.* **1993**, *347*, 31.
(28) Koper, M. T. M.; Sluyters, J. H. *J. Electroanal. Chem.* **1991**, *303*, 65.
(29) Krischer, K. Principles of Temporal and Spatial Pattern Formation in Electrochemical Systems. In *Modern Aspects of Electrochemistry*; White, R. E., Bockris, O. M., Conway, R. E., Eds.; Plenum: New York, 1995; Vol. 32; p 1.
(30) Mukouyama, Y.; Nakanishi, S.; Konishi, H.; Ikeshima, Y.; Nakato, Y. *J. Phys. Chem. B* **2001**, *105*, 10905.